Hydrogen recombination continuum as the radiative model for stellar optical flares

Paulo J. A. Simões[1,2]★, Alexandre Araújo[1], Adriana Valio[1], Lyndsay Fletcher[2,4]

[1]*Centro de Rádio Astronomia e Astrofísica Mackenzie, Escola de Engenharia, Universidade Presbiteriana Mackenzie, São Paulo, Brazil.*
[2]*SUPA School of Physics and Astronomy, University of Glasgow, Glasgow G12 8QQ, UK*
[3]*Rosseland Centre for Solar Physics, University of Oslo, PO Box 1029 Blindern, NO-0315 Oslo, Norway*

ABSTRACT

The study of stellar flares has increased with new observations from CoRoT, Kepler, and TESS satellites, revealing the broadband visible emission from these events. Typically, stellar flares have been modelled as 10^4 K blackbody plasma to obtain estimates of their total energy. In the Sun, white light flares (WLFs) are much fainter than their stellar counterparts, and normally can only be detected via spatially resolved observations. Identifying the radiation mechanism for the formation of the visible spectrum from solar and stellar flares is crucial to understand the energy transfer processes during these events, but spectral data for WLFs are relatively rare, and insufficient to remove the ambiguity of their origin: photospheric blackbody radiation and/or Paschen continuum from hydrogen recombination in the chromosphere. We employed an analytical solution for the recombination continuum of hydrogen instead of the typically assumed 10^4 K blackbody spectrum to study the energy of stellar flares and infer their fractional area coverage. We investigated 37 events from Kepler-411 and 5 events from Kepler-396, using both radiation mechanisms. We find that estimates for the total flare energy from the H recombination spectrum are about an order of magnitude lower than the values obtained from the blackbody radiation. Given the known energy transfer processes in flares, we argue that the former is a physically more plausible model than the latter to explain the origin of the broadband optical emission from flares.

Key words: stars: flare – stars: solar-type – radiation mechanisms: thermal

1 INTRODUCTION

Stellar magnetic activity manifests itself in a wide range of different phenomena. On the Sun, flares are high-energy events observed in the solar atmosphere. Solar flares are observed across the entire electromagnetic spectrum, such as radio, visible, ultraviolet, X-ray, and gamma rays. These transient phenomena occur in the solar atmosphere in regions of high magnetic field concentrations, where abundant amounts of energy are released in the corona by reconnection of the magnetic field (Benz 2017; Fletcher et al. 2011).

Solar flares are believed to be the result of the conversion of magnetic energy into particle kinetic energy. The energy released in flares is about 10^{27}–10^{32} erg, a large fraction of which is in the kinetic energy of accelerated, non-thermal electrons and ions, as estimated from hard X-ray and gamma-ray emission (e.g. Emslie et al. 2012; Warmuth & Mann 2020). Part of the released energy is radiated as thermal emission in soft X-rays from the corona, UV line and continuum emission from the chromosphere and from the transition region (chromosphere/corona), and white light (optical continuum) observed from the chromosphere or photosphere (see e.g. Milligan et al. 2014). Radio and millimeter emissions are also commonly detected during solar flares (Bastian et al. 1998; White et al. 2011), encouraging the development of instruments to cover the sub-millimetric range, such as the Solar Submillimeter Telescope (SST, Kaufmann et al. 2004, 2008), and adapting the Atacama Large Millimeter Array (ALMA) for solar observations (Wedemeyer et al. 2016; Bastian et al. 2022; Skokić et al. 2023). Therefore, observations with high temporal resolution images at all wavelengths are crucial to understanding the processes and mechanisms that occur in these complex (Benz & Güdel 2010). Solar white-light flares (WLFs), characterized by the enhancement of the optical continuum, have been extensively investigated, but often with poor spectral coverage, see e.g. Matthews et al. (2003) and Hudson et al. (2006). Early spectral observations, summarized by Hudson et al. (2010), indicated the presence or absence of the Balmer jump, indicating the presence or absence of a hydrogen free-bound (recombination) continuum, which led the community to label WLFs as type I and type II, respectively. A lack of conclusive observations meant that several models were proposed to explain the origin of the optical continuum and the formation of solar WLF (Boyer et al. 1985; Poland et al. 1988; Machado et al. 1989), including semi-empirical models based on observations (Machado et al. 1980; Mauas et al. 1990). In such works, one of the main points of discussion was related to the dominant mechanism producing the WL emission: a photospheric blackbody spectrum (BB) or a chro-

mospheric H free-bound continuum (Hfb). However, Hudson (1972) had already pointed out the difficulty of delivering the necessary energy, by accelerated electrons, into the photosphere to heat the local plasma and form a sufficiently hot blackbody spectrum to explain the WLF observations. An alternative is to heat the photosphere via illumination of UV lines formed in the chromosphere (backwarming) during flares (Machado et al. 1980), which also suffers from severe limitations (Poland et al. 1988; Simões et al. 2017).

In more recent spectral observations of solar WLFs, by Kerr & Fletcher (2014), Heinzel & Kleint (2014) and Kowalski et al. (2015b), once again both BB and Hfb models were compared, but without a definitive conclusion due to the poor spectral coverage or difficulties in obtaining an absolute calibration agreement between different instruments. Other methods were attempted to find the dominant mechanism forming the WLF emission. In the few cases where it was possible, investigations of the height of the white light emission in flares, with respect to the height of the hard X-ray (HXR) emission, were met with ambiguous results, placing the WL emission either at photospheric or mid-chromospheric heights (Martínez Oliveros et al. 2012; Krucker et al. 2015).

While solar-dedicated instruments with large spectral coverage and resolution are not currently available, Sun-as-a-star spectra are regularly obtained by the Low-Cost Solar Telescope (LCST) coupled with the High Accuracy Radial velocity Planet Searcher for the Northern hemisphere (HARPS-N). The solar spectra are used as a reference for physical processes that drive intrinsic stellar radial-velocity variations, which interfere with the search for exoplanets using radial-velocity methods (Collier Cameron et al. 2019; Milbourne et al. 2019; Pietrow et al. 2023). However, such instruments are not typically capable of detecting continuum enhancements during solar flares, given the low contrast of the emission, which is worsened by the integration of the emission of the full solar disk.

Dynamic models based on radiative-hydrodynamic simulations (RHD) have shown that ionization and recombination of hydrogen in the chromosphere are key factors governing the evolution of the flaring atmosphere (Abbett & Hawley 1999; Kowalski et al. 2015a; Simões et al. 2017). In particular, Simões et al. (2017) have shown that the dynamic process of ionization and recombination in the chromosphere, during the energy deposition phase, is fundamental in enhancing the local electron density and producing the mid-infrared (mid-IR) emission via free-free radiation (Ohki & Hudson 1975; Heinzel & Avrett 2012; Kašparová et al. 2009; Trottet et al. 2015). Solar flare observations in the mid-IR range are becoming more common (Kaufmann et al. 2013; Penn et al. 2016; Giménez de Castro et al. 2018; López et al. 2022; Giménez de Castro et al. 2020) and should help to place important constraints, both observational and theoretical, to identify the formation mechanism of WLFs in the Sun.

Flares are also a common energetic phenomenon in solar-type stars and M-dwarf stars. Stellar flares have been observed in radio (e.g. Bastian & Bookbinder 1987; Kundu et al. 1988) and millimetric wavelengths (MacGregor et al. 2018, 2020), optical and ultraviolet ranges (e.g. Hawley et al. 2007), and X-rays (e.g. Güdel & Nazé 2009). More recently, multi-wavelength observations of stellar flares have become more common (e.g. Howard et al. 2022; MacGregor et al. 2021; Namekata et al. 2023). The interpretation of the observations were often based on knowledge and models derived from solar flare analysis (e.g. Hawley et al. 2003; Maehara et al. 2015a), including RHD simulations (Allred et al. 2015; Kowalski et al. 2015a).

Kepler Space Telescope's high-precision photometry (Borucki et al. 2010) has enabled the systematic study of stellar flares, improving our understanding of stellar activity. With the emergence of such photometric data, it was possible to have a greater temporal cov-

erage of observations of stars (e. g. Davenport 2016). For example, Maehara et al. (2012) identified 365 superflares with energy on the order of 10^{33} to 10^{36} erg, based on 120 days of Kepler observations in 2009. These events were found in 148 G-type stars, where 14 events occurred in Sun-like stars. The results indicated that stars with superflares have an almost periodic variation in brightness, indicating the presence of very large starspots, and also that superflares in these Sun-like stars occur once every 800–5000 years (Shibayama et al. 2013). Following Kepler, the Transiting Exoplanet Survey Satellite (TESS, Ricker et al. 2014) has also contributed to the discovery and analysis of many more flares in active stars (e.g. Feinstein et al. 2020). An important contribution to studies of superflares was the estimation of the energy of such bursts. Many studies work with the assumption that the flare emission is originated from a blackbody plasma with $T = 10^4$ K, following the conclusions of Kretzschmar (2011).

In this paper, we propose an analytical form for the recombination continuum of hydrogen instead of the typically assumed 10^4 K blackbody spectrum to study the energy of stellar flares. The next section describes the data of two stars observed by the Kepler space mission. In Section 3, we detail the two proposed models for the stellar flares, whereas the results are compared in Section 4. Finally, the conclusions are presented in Section 5.

2 DATA

In this study, we use data from two stars: Kepler-411 and Kepler-396. The stellar parameters of both stars are listed in Table 1. The light curves of the two stars, Kepler-411 and Kepler-396, were retrieved from the MAST[1] data archive. We used short ($\approx$1 min) cadence data in the Pre-search Data Conditioning (PDCSAP) format for our analysis. There are 5 quarters of short cadence data for Kepler-411 (Q11 to Q17), and 6 quarters of Kepler-396 data (Q12 to Q17). The PDCSAP examines the calibrated light curves produced by photometric analysis and applies a series of corrections (including discontinuities, systematic trends, and outliers, such as cosmic rays) that obscure the astrophysical signals in the light curves. These corrections are based on known instrumental and spacecraft anomalies as well as unanticipated artifacts found in the data (Stumpe et al. 2012).

Kepler-411, a K2V star, was observed by the Kepler space telescope for about 600 days, exhibiting characteristics that indicate relatively strong magnetic activity (Sun et al. 2019). The activity of Kepler-411 was investigated in detail by Araújo & Valio (2021a) and Araújo & Valio (2021b).

Kepler-396, a G star, was observed by the Kepler Space Telescope for approximately 670 days. In the analysis of Kepler-396 light curves, we identified 5 flares, which characteristics as described in Table 2.

The identification of superflares in the Kepler-411 and Kepler-396 light curves was made using visual inspection of each quarter. Before performing a visual inspection of the light curves, we followed a few steps. Throughout the light curve, we checked and removed false data such as pointing errors, cosmic rays, and outliers. To remove the oscillatory trend due to the rotation of the spotted star from the light curve, a polynomial of degree three was applied and subtracted, and the relative flux of each flare with respect to the average flux of the star is obtained using Equation 2 of Hawley et al. (2014). Then, each quarter of the light curve was visually inspected and the superflares candidates were identified as three or more consecutive points with

---

[1] https://archive.stsci.edu/kepler/data_search/search.php

Table 1. Stellar parameters of Kepler-411 and Kepler-396.

Parameter	Stellar parameters	
	Kepler-411	Kepler-396
Spectral Type	K2V[a]	G[c]
Radius R_* [$R_\odot$]	0.820 ± 0.018[a]	$0.903^{+0.038}_{-0.036}$[c]
Mass [$M_\odot$]	0.87 ± 0.04[a]	0.81 ± 1.81[d]
Effective temperature $T_{\rm eff}$ [K]	4832[b]	5656 ± 113[c]
Period [days]	10.4 ± 0.03[a]	13.4 [e]

[a] (Sun et al. 2019); [b] (Gaia et al. 2018); [c] (Berger et al. 2018); [d] (Xie 2014); [e] (Maehara et al. 2015b).
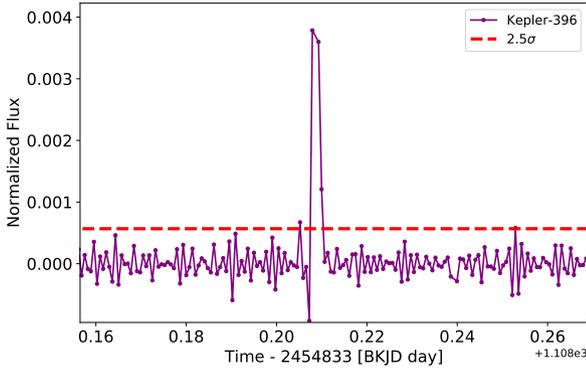
Figure 1. One of the superflares in Kepler-396 analyzed in this work, the first in Table 2. The lightcurve has been corrected for analysis and identification of flares and superflares (see Section 2). A sequence of three or more points above the 2.5σ threshold (red line) is considered a flare, as described in Araújo & Valio (2021a).

flux above the overall average flux by at least 2.5 standard deviations σ.

We analyzed 37 superflares on Kepler-411 previously analyzed by Araújo & Valio (2021b) and 5 superflares on Kepler-396, using the flare models described in Section 3. To identify the superflares of the star Kepler-396 (see Figure 1), we applied the same methodology as that used for Kepler-411, which was proposed by Araújo & Valio (2021b).

3 MODELS FOR THE OPTICAL FLARE EMISSION

3.1 Blackbody radiation

The blackbody specific intensity B_λ at wavelengths λ is

$$B_\lambda(T) = \frac{2hc^2}{\lambda^5}\left[\exp\left(\frac{hc}{\lambda k_B T}\right) - 1\right]^{-1} \tag{1}$$

where h is the Planck constant, c is the speed of light, k_B is the Boltzmann constant, T is the temperature of the blackbody. For the quiescent stellar emission, T is defined as the effective temperature of the star $T_{\rm eff}$. For the flare emission under the blackbody assumption, we set $T = 10^4$ K, following the usual assumption made in the recent literature (e.g. Maehara et al. 2012). We also modelled our sample of flares using a blackbody with $T = 6642$ K, which gives the same total energy output as the adopted H recombination spectrum (see Section 3.2).

Under these assumptions, the emitting area $A_f(t)$ of an observed

event can be estimated by

$$A_f(t) = C_f(t)\pi R_*^2 \frac{\int R_\lambda B_\lambda(T_*)d\lambda}{\int R_\lambda B_\lambda(T_f)d\lambda} \tag{2}$$

where R_* is the radius of the star, R_λ is the spectral response of the telescope[2] and $C_f(t)$ is the relative luminosity of the flare (i.e. the observed quantity obtained from Kepler data):

$$C_f(t) = \frac{L_f(t)}{L_*}. \tag{3}$$

It then follows that the flare luminosity $L_f(t)$ can be estimated by using the Stefan-Boltzmann law

$$L_f(t) = \sigma T_f^4 A_f(t) \tag{4}$$

where σ is the Stefan-Boltzmann constant, and $A_f(t)$ is the flare emitting area, and the total radiated energy can be found by

$$E_f = \int_{t_0}^{t_f} L_f(t)dt \tag{5}$$

where the time integral is done for the duration of the flare.

3.2 Hydrogen free-bound radiation

Following Kerr & Fletcher (2014) and references therein, we assume a simple optically thin slab of plasma with a physical thickness L, with isothermal temperature T_c and uniform electron density n_e. This slab is located above the photosphere and no radiation backwarming is considered. Under these assumptions, the hydrogen free-bound specific intensity (in erg s^{-1} cm^{-2} Å^{-1} sr^{-1}) can be calculated by (Aller 1963)

$$I_\lambda = \left(\frac{6.48 \times 10^{-14}}{4\pi\lambda^2}\right)\left(\frac{T_c^{-3/2}}{n^3}\right)\exp\left(\frac{1.48 \times 10^5}{n^2 T_c} - \frac{1.44 \times 10^8}{\lambda T_c}\right)n_e^2 L \tag{6}$$

where λ is the wavelength in Å, n_e is the electron density in cm^{-3}, T_c is the temperature in K, L is the thickness of the slab in cm, n is the principal quantum number of the energy level in the hydrogen atom to which the electron recombines. For the wavelength covered by Kepler observations, we consider $n = 3$ (Paschen) and $n = 4$ (Brackett). In this work, we adopt $T_c = 10^4$ K in line with the findings of Kretzschmar (2011), and $n_e^2 L = 5 \times 10^{35}$ cm^{-5}. For reference, Kerr & Fletcher (2014) found $n_e^2 L \approx 7 \times 10^{34}$ cm^{-5} for the solar flare SOL2011-02-15. As noted by Kerr & Fletcher (2014), Eq. 6 assumes ionisation equilibrium, a Maxwellian velocity distribution, a pure hydrogen plasma, and the Gaunt factor is ≈ 1. Hence, the interpretation of the results are only valid under these assumptions. We note that Machado et al. (2018), analyzing solar flare observations of the Lyman continuum (using data from the *Extreme ultraviolet Variability Experiment* (EVE, Woods et al. 2012), have suggested that the flaring chromospheric plasma approaches LTE conditions, supporting our adoption of the LTE assumption. A more detailed evaluation of the equilibrium assumption could be done with RHD modelling, which can handle the dynamics of ionisation and recombination during the energy deposition phase, but this is beyond our scope in this work.

Employing this radiation model to analyse the observational data

---

[2] The Kepler Space Telescope response function (Van Cleve & Caldwell 2016) is available at https://keplerscience.arc.nasa.gov/the-kepler-space-telescope.html
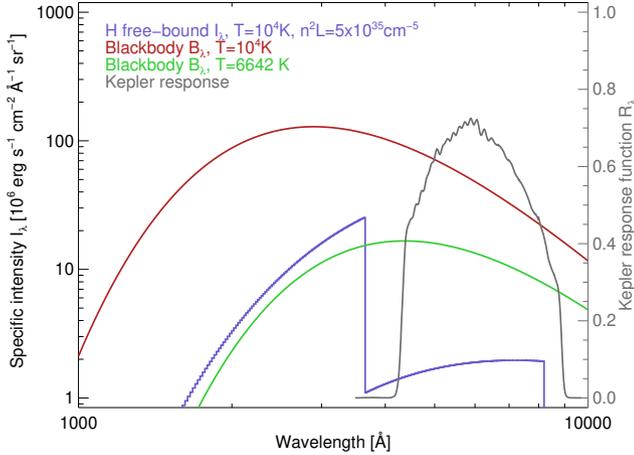
Figure 2. Flare spectral models adopted in this work: blackbody model with $T = 10^4$ K (red) and $T = 6642$ K (green), and the H free-bound model with $T = 10^4$ K and $n^2 L = 5 \times 10^{35}$ cm^{-5} (blue). The Kepler response function is also shown (gray).

is straightforward; once I_λ is calculated, we use Eq. 2, replacing $B_\lambda(T_f)$ with I_λ, to obtain the flaring area $A_f(t)$. The flare luminosity $L_{f,\text{Hfb}}$ in this case is found by

$$L_{f,\text{Hfb}} = A_f(t)\pi \int_0^\infty I_\lambda d\lambda, \qquad (7)$$

and by performing the time integral (Eq. 5) with $L_{f,\text{Hfb}}$ for the duration of the event, we obtain the total radiated energy $E_{f,\text{Hfb}}$. Note that in the following sections, we present and discuss the maximum of the relative flare area $A_f(t)/(\pi R_*^2)$, i.e. the area associated with the maximum relative flux observed, for each flare. The resulting flare models are shown, along with the Kepler response function, in Figure 2.

4 RESULTS AND DISCUSSION

Our results, displayed in Figure 3, show that the Hfb model requires larger areas than the BB model (about one order of magnitude larger) and that it radiates less energy ($\approx 20\%$) than the BB at 10^4K model. The Hfb model is a less efficient mechanism to radiate the energy away from the flaring atmosphere, compared to a BB at 10^4K. Nevertheless, the Hfb model still yields total energy values compatible with the superflare category. The larger relative areas inferred from the Hfb model do not impose a strong constraint for the adoption of this model since spot group areas in active stars are likely to cover up at least 1% of the surface of the star (Notsu et al. 2013; Okamoto et al. 2021).

The BB model at 6642 K yields flare areas about half the size inferred from the Hfb model, for the same output energy as expected, since the temperature of 6642 K was chosen to result in the same total energy provided by the Hfb model. This exercise was performed to demonstrate that the temperature chosen for the BB model is often arbitrary, but not without an important impact on the derived parameters for the observed flares, such as the relative emitting area. The parameters for the Hfb model, namely the chromospheric temperature and emission measure $n_e^2 L$, are more constrained in nature since the thickness L of the emitting layer and its hydrogen density n_e^2 will be limited by the characteristics of the chromosphere of
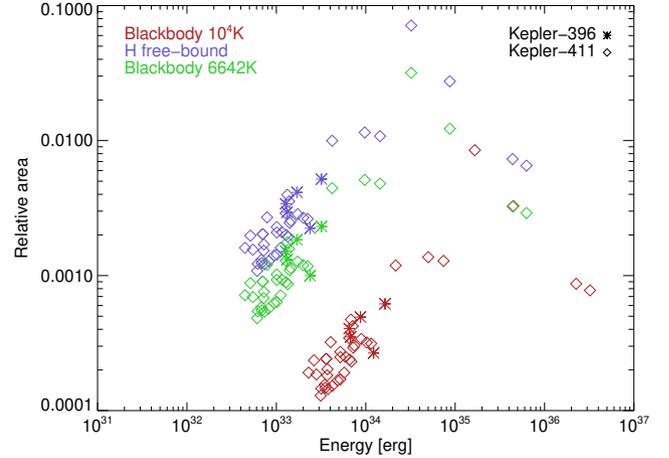
Figure 3. Relative area versus total energy of flares from Kepler-411 (diamonds) and Kepler-396 (asterisks) stars, modelled as blackbody with $T = 10^4$ K (red symbols), H free-bound continuum (blue symbols), and blackbody at $T = 6642$ K (green symbols). The latter refers to a BB model that gives the same total energy as the Hfb model. Therefore, the energy estimates for the flares from the Hfb and BB at 6642 K models are the same. However, Hbf needs a larger area because Kepler would not see a large part of the Hfb spectrum (Balmer continuum), in comparison with the BB with 6642 K.

the star (thickness, density, and temperature), allowing for narrow possibilities for these parameters. From this, it follows that the flare areas inferred from this model vary less with the choice of the model parameters than in the case of a BB model.

Our main argument in favor of the Hfb model instead of the BB model is based on the physics of the flaring atmosphere. The ubiquity of HXR and microwave emission in solar flares has consolidated the presence of accelerated electrons as part of the physical processes in these events (Fletcher et al. 2011; White et al. 2011). These electron beams are commonly considered as the main process to transfer the energy released from the magnetic field into the lower atmosphere, triggering the response of the chromospheric plasma. If a similar process occurs in stellar flares, as is likely the case, the accelerated electrons cannot easily penetrate into the photosphere, instead being collisionally stopped in the chromosphere, where they deposit their energy excess (Hudson 1972; Hawley & Fisher 1992; Allred et al. 2015). Even if the energy can be deposited in the photosphere of the active star (by an unknown mechanism), and an originally neutral hydrogen plasma were to be heated up to 10^4 K, the hydrogen should ionize, and if an equilibrium is maintained during the flare, the recombination continuum (Hfb) should also contribute to the flare emission.

The backwarming mechanism, often regarded as a possible way to heat the photosphere, relies on the formation of UV lines above the photosphere. Earlier calculations by Poland et al. (1988) suggested that backwarming illumination is not sufficient to heat the photosphere to produce WLFs. Reinforcing this conclusion, more recent RHD simulations of flares, using the RADYN code (Allred et al. 2015), do not show any changes at photospheric depths under typical flare conditions (e.g. Simões et al. 2017; Kerr et al. 2019a,b, 2021).

When estimating superflare energy values, careful attention should be given to errors. This estimation of E_f is influenced by various types of uncertainties. Errors in stellar effective temperature (T_{eff}) and stellar radius (R) typically affect E_f values by approximately

3% and 7%, respectively ([Gaia et al. 2018](#)). Determination of errors in flare start/end times and quiescent levels also impact the flare amplitude values and, consequently, E_f values, typically by around 30%. We note, however, that these uncertainties affect the results of both models assumed here, and thus, do not interfere with the overall conclusions of this work.

The simple Hfb model proposed here does not take into account non-thermal ionisation of hydrogen atoms, i.e. by accelerated electrons ([Fang et al. 1993](#)), which would allow for the enhancement of the free-bound continuum at temperatures below the ionisation threshold. Likewise, non-LTE effects and the dynamical evolution of the flaring atmosphere should also affect the development of the optical continuum ([Allred et al. 2015](#)).

Another factor to consider is the variations in the flaring atmosphere during WLFs. Similarly, such variations can also pose challenges in estimating the energy of superflares, in particular under the assumption of a BB model. In the [Namekata et al. (2017)](#) study, the blackbody temperature of flare emissions changes to 6000-7000K, which can result in a 50% variation in flare energy. Likewise, the chromospheric density and/or the thickness of the emitting layer is likely to vary during flares, and thus, the Hfb spectrum should vary accordingly. Furthermore, since both stellar quiescent radiation and flare emissions may not exhibit complete blackbody radiation, flare energy values (derived under a blackbody assumption) may have an error of a few tens of percent ([Okamoto et al. 2021](#)). Moreover, we are neglecting the presence of spectral lines in emission during flares in this analysis, but we note that they must also have some contribution to the total radiation detected by broadband photometers such as Kepler and TESS.

[Maehara et al. (2015a)](#), analysing 187 superflares on 23 solar-type stars, found a positive correlation between flare energy and spot area (Fig. 5 of their paper), with spot areas covering up to 10% of the stellar disk. While Maehara et al. adopted a BB flare model, a Hfb model (as presented here) would yield ≈ 10 times less energy, while the flare areas would still fall within the spot areas. As a consequence, the Hfb model suggests a lower requirement for the stored magnetic energy necessary to power a flare.

We also note that center-to-limb effects, i.e. variations in the observed flare intensity as a function of its location in the solar or stellar disk, may affect the emission depending on the radiation mechanism. For instance, it my have strong effects for spectral lines during flares (e.g. [Capparelli et al. 2017](#); [Otsu et al. 2022](#); [Pietrow & Pastor Yabar 2023](#)). If the adopted model is a photospheric blackbody emission, then a limb-darkening effect should be accounted for, if the flare location is known - an easy task for solar flare analysis, but a difficult one for stellar flares. In the case of the chromospheric hydrogen recombination continuum model, however, such an effect might not be too relevant, although a proper radiative transfer calculations should be performed to quantify it. In any case, the parameter space of the relevant quantities (such as the electron beam parameters) should create much larger variations in the resulting spectra than the center-to-limb effects.

5 CONCLUSIONS

In this study, we propose the adoption of the hydrogen recombination (free-bound, Hfb) spectrum as a model for stellar flares, and present a comparison with the typical model employed for this purpose, a blackbody (BB) spectrum at $T = 10^4$ K. We analyzed 37 superflares on the star Kepler-411 by [Araújo & Valio (2021b)](#) and 5 superflares

on the star Kepler-396, applying both models to estimate the total flare energy and relative flare area.

We find the the Hfb model yields total flare energy estimates a factor of ≈ 10 times smaller than the BB at $T = 10^4$ K model, while requiring flare areas about 5 times larger. The inferred flare areas are still in agreement with values found by other authors and also within the estimates of spot group areas ([Notsu et al. 2013](#); [Okamoto et al. 2021](#)).

From a physical perspective, we strongly suggest the adoption of the Hfb model instead of the BB at $T = 10^4$ K model. Based on decades of observations of solar flares, and models proposed to explain these observations, the bulk of the energy deposition occurs in the chromosphere. There, the predominantly neutral hydrogen can be easily ionized during flares, and it is maintained in a dynamical equilibrium, generating the Hfb continuum that should dominate over any contribution from a slightly heated photosphere - which can only marginally happen via backwarming from UV emission formed in the chromosphere.

We strongly encourage the development of new dedicated spectrometers with high enough spectral resolution, sensitivity, and band coverage (3000 to 6000 Å) to capture the WL emission for solar flares, and provide the much needed observational constraints for the models.

DATA AVAILABILITY

The reduced data analyzed in this article is available upon request.

REFERENCES

Abbett W. P., Hawley S. L., 1999, ApJ, 521, 906
Aller L. H., 1963, Astrophysics. The atmospheres of the sun and stars. The Ronald Press Company
Allred J. C., Kowalski A. F., Carlsson M., 2015, ApJ, 809, 104
Araújo A., Valio A., 2021a, ApJ, 907, L5
Araújo A., Valio A., 2021b, ApJ, 922, L23
Bastian T. S., Bookbinder J. A., 1987, Nature, 326, 678
Bastian T. S., Benz A. O., Gary D. E., 1998, ARA&A, 36, 131
Bastian T. S., Shimojo M., Bárta M., White S. M., Iwai K., 2022, Frontiers in Astronomy and Space Sciences, 9, 977368
Benz A. O., 2017, Living Reviews in Solar Physics, 14, 2
Benz A. O., Güdel M., 2010, Annual Review of Astronomy and Astrophysics, 48, 241
Berger T. A., Huber D., Gaidos E., van Saders J. L., 2018, The Astrophysical Journal, 866, 99

Table 2. Parameters of Superflares in Kepler-396.

Start [BJD]	Stop [BJD]	Duration [Min]	Rise time [Min]	Decay time [Min]	Peak Time [BJD]
1108.20725	1108.22087	19.6156	2.94192	16.6737	1108.20928
1207.64762	1207.66193	20.5977	6.86592	13.7318	1207.65239
1337.49850	1337.51552	24.5203	3.92400	20.5963	1337.50122
1491.52902	1491.53992	15.6916	3.92256	11.7691	1491.53175
1532.26988	1532.27873	12.7512	2.94192	9.80928	1532.27192

Borucki W. J., et al., 2010, Science, 327, 977

Boyer R., Sotirovsky P., Machado M. E., Rust D. M., 1985, Sol. Phys., 98, 255

Capparelli V., et al., 2017, ApJ, 850, 36

Collier Cameron A., et al., 2019, MNRAS, 487, 1082

Davenport J. R. A., 2016, ApJ, 829, 23

Emslie A. G., et al., 2012, ApJ, 759, 71

Fang C., Henoux J. C., Gan W. Q., 1993, A&A, 274, 917

Feinstein A. D., Montet B. T., Ansdell M., Nord B., Bean J. L., Günther M. N., Gully-Santiago M. A., Schlieder J. E., 2020, AJ, 160, 219

Fletcher L., et al., 2011, Space Sci. Rev., 159, 19

Gaia C., et al., 2018, Astronomy & Astrophysics, 616

Giménez de Castro C. G., Raulin J. P., Valle Silva J. F., Simões P. J. A., Kudaka A. S., Valio A., 2018, Space Weather, 16, 1261

Giménez de Castro C. G., et al., 2020, Sol. Phys., 295, 56

Güdel M., Nazé Y., 2009, A&ARv, 17, 309

Hawley S. L., Fisher G. H., 1992, ApJS, 78, 565

Hawley S. L., et al., 2003, ApJ, 597, 535

Hawley S. L., Walkowicz L. M., Allred J. C., Valenti J. A., 2007, PASP, 119, 67

Hawley S. L., Davenport J. R., Kowalski A. F., Wisniewski J. P., Hebb L., Deitrick R., Hilton E. J., 2014, The Astrophysical Journal, 797, 121

Heinzel P., Avrett E. H., 2012, Sol. Phys., 277, 31

Heinzel P., Kleint L., 2014, ApJ, 794, L23

Howard W. S., et al., 2022, ApJ, 938, 103

Hudson H. S., 1972, Sol. Phys., 24, 414

Hudson H. S., Wolfson C. J., Metcalf T. R., 2006, Sol. Phys., 234, 79

Hudson H. S., Fletcher L., Krucker S., 2010, Mem. Soc. Astron. Italiana, 81, 637

Kaufmann P., et al., 2004, ApJ, 603, L121

Kaufmann P., et al., 2008, in Stepp L. M., Gilmozzi R., eds, Society of Photo-Optical Instrumentation Engineers (SPIE) Conference Series Vol. 7012, Ground-based and Airborne Telescopes II. p. 70120L, doi:10.1117/12.788889

Kaufmann P., et al., 2013, ApJ, 768, 134

Kašparová J., Heinzel P., Karlický M., Moravec Z., Varady M., 2009, Central European Astrophysical Bulletin, 33, 309

Kerr G. S., Fletcher L., 2014, ApJ, 783, 98

Kerr G. S., Carlsson M., Allred J. C., Young P. R., Daw A. N., 2019a, ApJ, 871, 23

Kerr G. S., Allred J. C., Carlsson M., 2019b, ApJ, 883, 57

Kerr G. S., Xu Y., Allred J. C., Polito V., Sadykov V. M., Huang N., Wang H., 2021, ApJ, 912, 153

Kowalski A. F., Hawley S. L., Carlsson M., Allred J. C., Uitenbroek H., Osten R. A., Holman G., 2015a, Sol. Phys.,

Kowalski A. F., Cauzzi G., Fletcher L., 2015b, ApJ, 798, 107

Kretzschmar M., 2011, Astronomy & Astrophysics, 530, A84

Krucker S., et al., 2015, ApJ, 802, 19

Kundu M. R., Pallavicini R., White S. M., Jackson P. D., 1988, A&A, 195, 159

López F. M., Giménez de Castro C. G., Mandrini C. H., Simões P. J. A., Cristiani G. D., Gary D. E., Francile C., Démoulin P., 2022, A&A, 657, A51

MacGregor M. A., Weinberger A. J., Wilner D. J., Kowalski A. F., Cranmer S. R., 2018, ApJ, 855, L2

MacGregor A. M., Osten R. A., Hughes A. M., 2020, ApJ, 891, 80

MacGregor M. A., et al., 2021, ApJ, 911, L25

Machado M. E., Avrett E. H., Vernazza J. E., Noyes R. W., 1980, ApJ, 242, 336

Machado M. E., Emslie A. G., Avrett E. H., 1989, Sol. Phys., 124, 303

Machado M. E., Milligan R. O., Simões P. J. A., 2018, ApJ, 869, 63

Maehara H., et al., 2012, Nature, 485, 478

Maehara H., Shibayama T., Notsu Y., Notsu S., Honda S., Nogami D., Shibata K., 2015a, Earth, Planets and Space, 67, 59

Maehara H., Shibayama T., Notsu Y., Notsu S., Honda S., Nogami D., Shibata K., 2015b, Earth, Planets and Space, 67, 59

Martínez Oliveros J.-C., et al., 2012, ApJ, 753, L26

Matthews S. A., van Driel-Gesztelyi L., Hudson H. S., Nitta N. V., 2003, A&A, 409, 1107

Mauas P. J. D., Machado M. E., Avrett E. H., 1990, ApJ, 360, 715

Milbourne T. W., et al., 2019, ApJ, 874, 107

Milligan R. O., et al., 2014, ApJ, 793, 70

Namekata K., et al., 2017, The Astrophysical Journal, 851, 91

Namekata K., et al., 2023, arXiv e-prints, p. arXiv:2311.07380

Notsu Y., et al., 2013, ApJ, 771, 127

Ohki K., Hudson H. S., 1975, Sol. Phys., 43, 405

Okamoto S., Notsu Y., Maehara H., Namekata K., Honda S., Ikuta K., Nogami D., Shibata K., 2021, The Astrophysical Journal, 906, 72

Otsu T., Asai A., Ichimoto K., Ishii T. T., Namekata K., 2022, ApJ, 939, 98

Penn M., Krucker S., Hudson H., Jhabvala M., Jennings D., Lunsford A., Kaufmann P., 2016, ApJ, 819, L30

Pietrow A. G. M., Pastor Yabar A., 2023, arXiv e-prints, p. arXiv:2311.06200

Pietrow A. G. M., et al., 2023, arXiv e-prints, p. arXiv:2309.03373

Poland A. I., Milkey R. W., Thompson W. T., 1988, Sol. Phys., 115, 277

Ricker G. R., et al., 2014, in Oschmann Jacobus M. J., Clampin M., Fazio G. G., MacEwen H. A., eds, Society of Photo-Optical Instrumentation Engineers (SPIE) Conference Series Vol. 9143, Space Telescopes and Instrumentation 2014: Optical, Infrared, and Millimeter Wave. p. 914320 (arXiv:1406.0151), doi:10.1117/12.2063489

Shibayama T., et al., 2013, The Astrophysical Journal Supplement Series, 209, 5

Simões P. J. A., Kerr G. S., Fletcher L., Hudson H. S., Giménez de Castro C. G., Penn M., 2017, A&A, 605, A125

Skokić I., Benz A. O., Brajša R., Sudar D., Matković F., Bárta M., 2023, A&A, 669, A156

Stumpe M. C., et al., 2012, Publications of the Astronomical Society of the Pacific, 124, 985

Sun L., Ioannidis P., Gu S., Schmitt J., Wang X., Kouwenhoven M., 2019, A&A, 624, A15

Trottet G., et al., 2015, Sol. Phys., 290, 2809

Van Cleve J. E., Caldwell D. A., 2016, Kepler Instrument Handbook, Kepler Science Document KSCI-19033-002

Warmuth A., Mann G., 2020, A&A, 644, A172

Wedemeyer S., et al., 2016, Space Sci. Rev., 200, 1

White S. M., et al., 2011, Space Sci. Rev., 159, 225

Woods T. N., et al., 2012, Sol. Phys., 275, 115

Xie J.-W., 2014, The Astrophysical Journal Supplement Series, 210, 25

This paper has been typeset from a TeX/LaTeX file prepared by the author.